Communications on Applied Nonlinear Analysis
ISSN: 1074-133X
Vol 32 No. 9s (2025)

Structural Study of ZnO Nanostructures on Porous Silicon: Effect of Precursor Molarity

Kevin Alvin Eswar[a,b,c,*] , Muliyadi Gulilling[a,b] , Husairi Fadzilah Suhaimi[b,c] , Zuraida Khusaimi[b,c], Rusop Mahmood[c], Saifollah Abdullah[b,c]

[a]Faculty of Applied Sciences, Universiti Teknologi MARA Sabah Branch Tawau Campus Tawau, Malaysia *Email: kevinalvin86@gmail.com

[b]Faculty of Applied Sciences, Universiti Teknologi MARA Shah Alam, Shah Alam, Malaysia

[c]Nano SciTech Centre, Institute of Science, Universiti Teknologi MARA Shah Alam, Shah Alam, Malaysia

Article History:
Received: 12-01-2025
Revised: 15-02-2025
Accepted: 01-03-2025

Abstract:
Wet colloid chemical approach has been employed to synthesis ZnO Nanostructure on Porous Silicon (PSi). Precursor molarities in the range of 0.01 M to 0.20 M were used in order to study its effect on structural property of ZnO nanostructures. Field emission scanning electron microscopy (FESEM) was used to investigate the surface morphology. The result shows that the formation of flower-like composed of nano-particles at 0.01 M. Flower-like ZnO with hexagonal structures were seen at molarity of 0.20 M. The structural was characterized using X-ray diffraction (XRD) microscopy. XRD Spectra shows the peak of (100), (002) and (101) were clearly seen as dominant peaks. In addition, peaks of (102) and (110) are also appeared. The crystallite sizes were in range of 37.9 to 54 nm. Zn-O of 0.19 nm was obtained from the XRD spectra analysis. Based on the texture coefficient analysis, crystalline of ZnO grew with plane (002)-oriented.

Keywords: Structural properties; hydrothermal method; ZnO nanostructures

1 Introduction

Zinc Oxide (ZnO) is a versatile semiconductor with various applications. Basically, ZnO has two stable crystalline structures, hexagonal wurtzite and cubic blende. The hexagonal wurtzite is more stable at ambient temperature [1]. The large binding energy of 60 meV and wide energy band gap of 3.37 eV in room temperature make it widely applied in sensor, photodetector, light emitting devices and UV detectors. In addition, M. Shaban et. al have coating ZnO nanoparticle on fabrics to enhance their superhydrophobic and antibacterial properties [2]. There are several methods have been used to produce ZnO nanostructure such as radio frequency magnetron sputtering, chemical vapour deposition, spin coating method, hydrothermal method, pulsed laser deposition and spray pyrolysis [3-7]. Among them, hydrothermal deposition was widely choosen as the simplest, easy to control and low-cost method. Various structures of ZnO have been produced suc as flower-like, nanoparticles, nanowire and nanorods. These structures were highly depending on method and parameter during the deposition process. Selection of substrate depends on its application. Glass for photodetecter [8], silicon for sensor [9], mild steel as anti-corrotion [10] and fabrics for antibacterial [2] have been chosen in the previous studies. In this work ZnO nanostructure deposited on PSi via hydrothermal method.

2 Methodology

2.1 Substrate Preparation

Silicon was cleaned using acetone, methanol and dilute acid prior to etching process. Then, the polished side of silicon surface was etched using electrochemical etching method to form porous silicon (PSi). Then, the PSi surface was coated by ZnO thin films using spin coating method as a seed layer.

2.2 Deposition of ZnO Nanostructures

Zinc nitrate hexahydrate ($Zn(NO_3)_2.6H_2O$) was used as starting material while hexamethylenetetramine (HMTA) as a stabilizer and deionized water as a solvent. The molarities of precursor were varied in the range of 0.01 M to 0.2 M. PSi substrate was immersed into the ZnO precursor at 90 ℃ for 4 hours. It was followed by post-annealing heat treatment at 500℃.

2.3 Characterizations

The field emission scanning microscopic (FESEM) was used to study the morphology of ZnO nanostructures. The structural properties was investigated using X-ray diffraction (XRD) **s**pectroscopy.

3 Results and Discussion

Figure 1 shows the FESEM images of ZnO nanostructures at molarity 0.01 M, 0.05 M and 0.20 M. Low concentration produced flower-like composed of nanoparticles. Nanoparticles with sizes ranging from 20 nm to 40 nm were produced on a large scale at a concentration of 0.01 M. Then, flower-like ZnO composed of microrods appeared at molarity 0.05 M. Nanoparticles were still clearly seen on top of the microrods. Flower-like ZnO composed of dense and packed ZnO microrods with diameter ranging from 400 nm to 700 nm formed at 0.20 M. The diameter of microrods in the flower-like structures uniformly increased with increasing solution concentration. The number of Zinc ion highly influences the number of ZnO colloidal or ZnO nuclei formation. It means concentration is very sensitive parameter where different molarity has different amount of zinc ion within the solution.

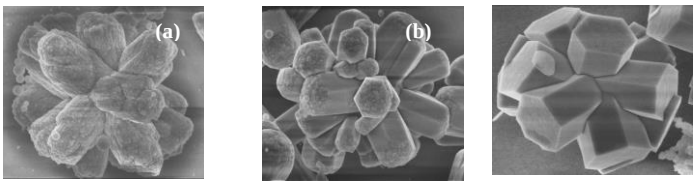

Figure 1. FESEM images of ZnO nanostructures at molarity (a) 0.01 M, (b) 0.05 M and (c) 0.20 M

XRD patterns of ZnO nanostructures with different solution concentrations of 0.01 M, 0.05 M, 0.1 M and 0.20 M were analyzed to explore the influence on structural on ZnO nanostructures. **Figure 2** shows the XRD pattern of ZnO nanostructures synthesized in different molarity of precursor. Several diffraction peaks were observed in the spectra of the samples from 30° to 60°. Peak of (100), (002), (101), (102) and (110) correspond to hexagonal ZnO wurtzite can be observed apparently (JCPDS

No: 36-1451). Besides, peak of impurity corresponds to silicon is also appearing in between of plane (100) and (002) for all samples (JCPDS No: 17-0901).

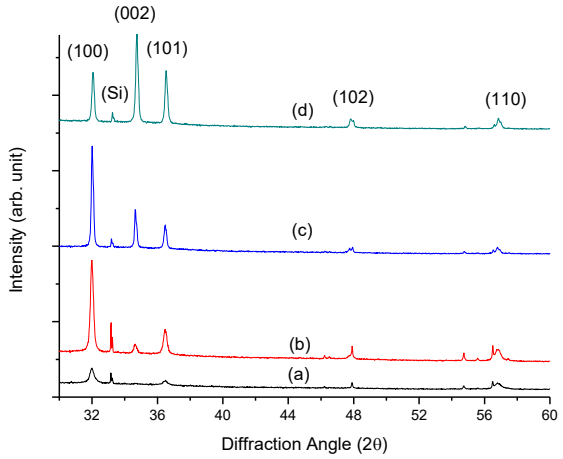

Figure 2. XRD of ZnO nanostructures in different molarity of (a) 0.01 M, (b) 0.05 M, (c) 0.10 M and (d) 0.20 M

Table 1 shows the peak position, intensities and full width at half maximum (FWHM) of plane (002) in different molarities. In this study, plane (002) will be discussed in details. Plane (002) of 0.01 M shows that the peak position at 34.70 °. It was shifted to lower diffraction angle at molarity of 0.05 M, maintained at molarity of 0.10 M. Then, the peak position shifted to higher diffraction angle of 34.74 °.Suggested that, diffraction angle was shifted due to effect of stress or imperfection of the crystalline of ZnO nanostructures [11, 12]. As shown in Table 4.5, the intensity of all peaks generally increases when molarity of precursor increased. The (002)-oriented peak relatively increased with increasing molarities of the precursor, which indicated that the preferred growth orientation of the grown ZnO nanostructures is toward the *c*-axis. *This result can be* attributed *to* the low surface free energies of the (002) plane [13]. According to the crystal behavior, a typical wurtzite ZnO crystal has non-polar faces, and (002) planes have polar faces. The ZnO wurtzite known that in c-axis oriented ZnO, there is a dipole moment perpendicular to the ZnO surface terminating with the (001) basal plane either a Zn plane or an O plane, both slightly charged. In this study, plane of (100) is another preferred orientation. However, in a-axis-oriented ZnO, the growing surface is terminated by lateral planes such as (100) planes. However the lateral planes in crystals with wurtzite structure are not electrically charged because the Zn and the O atoms in equal number occupy alternating position. So, these planes have a much lower surface energy, resulting in a smooth surface. In general, XRD peak intensity is strongly dependent on the ZnO film thickness. However, the relative intensity of the ZnO (100) diffraction peak decreases with increasing precursor concentration. A similar result of decreased intensity of the diffraction peak was reported by Kim et al. [14].

TABLE 1: Peak position, intensities and FWHM of plane (002) in different molarities

Molarity (M)	Peak position (2θ)	FWHM (°)
0.01	34.70	0.195

0.05	34.65	0.219
0.10	34.65	0.154
0.2	34.74	0.169

The initial stage of ZnO thin film growth, the large structural mismatch between ZnO nanostructures and the substrate in a large strain in the ZnO thin films, so the growth of the ZnO thin films is disturbed. As the ZnO thin films grow thicker, the strain between the newly grown ZnO layer and the former layer reduced; thus, the thicker thin films on substrate surface usually exhibit narrower FWHM of the diffraction peak and better crystal quality [14]. An estimation of crystallite size, *D* based on plane distance for each plane is also calculated. Equation (1) shows the Bragg's equation which used to calculate the plane distance for each plane. The parameter of λ, *d*, and θ represents sources wavelength, plane distance and peak position in radian. In this study, 0.154 nm of Cu Kα radiation was used as sources [12].

$$\lambda = 2d\sin\theta \quad (1)$$

Scherrer's formula was used to estimate the crystalline size by using plane distance, *d* for each plane. It can be represented by

$$D = \frac{K\lambda}{\beta cos\theta} \quad (2)$$

where *D, K,* λ*,* β*,* and θ represents crystallite size, Schrrer's constant (0.9), X-ray wavelength, FWHM and peak position respectively [15]. This equation shows that crystallite size, *D* is directly influenced by the FWHM and peak position of each plane. Generally, based on (002) plane, the size increase when the molarity increased from 0.01 M to 0.10 M. However, the size decreased at molarity of 2.0 M. Plane of (002) were considered because its FWHM is the smallest while the intensity the highest. The size of 49.17 nm was consistent with crystallite size obtained by Kim et. al. [15]

TABLE 2: Plane distance, *d* and crystallite size based on plane (002) in different molarities

Molarity (M)	**Plane distance, *d* (nm)**	**Crystallite Size, *D* (nm)**
0.01	0.2581	42.60
0.05	0.2585	37.86
0.10	0.2585	54.09
0.2	0.2578	49.17

Table 3 shows the lattice constant of '*a'* and '*c'*, Zn-O bond length, *L* and *u*, parameter used in bond length calculation in various molarity. As a reference, lattice constant of ZnO from JCPDS 36-1451 are a_0=b_0= 0.32498 nm and c_0=0.52066 nm. Lattice constant of '*a*' and '*c*' of the ZnO wurtzite structure can be calculated using the relation [12]

$$\frac{1}{d^2{}_{hkl}} = \frac{4}{3}\left(\frac{h^2+hk+k^2}{a^2}\right) + \frac{l^2}{c^2} \quad (3)$$

where d_{hkl} represents distance between adjacent planes in the Miller indices (*hkl*). Parameter of '*a'* and *'c'* are the lattice constant. The lattice constant '*a'* is obtained from plane (100) with relation

$$\frac{1}{d^2{}_{100}} = \frac{4}{3}\left(\frac{1}{a^2}\right) \quad (4)$$

while, the lattice constant '*c*' can be obtained from plane (002) with relation

$$\frac{1}{d^2{}_{002}} = \frac{4}{c^2} \quad (5)$$

From Equation (1), (4) and (5), the lattice constant '*a*' and '*c*' can be derived as

$$a = \frac{\lambda}{\sqrt{3}\sin\theta} \quad (6)$$

$$c = \frac{\lambda}{\sin\theta} \quad (7)$$

In order to find the bond length, *L* of Zn-O, lattice parameter 'a' and 'c' were used in the relation [16]

$$L = \sqrt{\left(\frac{a^2}{3} + \left(\frac{1}{2} - u\right)^2 c^2\right)} \quad (8)$$

where,

$$u = \frac{a^2}{3c^2} + 0.25 \quad (9)$$

As can be seen in the **Table 3**, lattice parameter 'a' and 'c' are consistent in all samples. It was found that the value 'a' and 'c' are 0.32 nm and 0.52 respectively. It is no affected by the molarity of precursor. Based on equation (8), bond length, *L* is highly dependent on lattice parameter. So, Zn-O

bond lengths of 0.196 nm are found for all samples. This value is consistent with Kim et al. findings [16].

TABLE 3: Lattice constant and bond length, *L* of ZnO nanostructurs on PSi

Molarity (M)	**Lattice constant (nm)**	**Bond Length, *L* (nm)**
0.01	a = 0.3225 c = 0.5163	0.19
0.05	a = 0. 3225 c = 0.5170	0.19
0.10	a = 0.3225 c = 0.5170	0.19
0.2	a = 0.3225 c = 0.5155	0.19

Figure 3 show the texture coefficient, *TC* of peak (100), (002) and (101). In order to calculate the texture coefficient, *TC* following equation was used [17].

$$TC_{(hkl)} = \frac{\frac{I_{(hkl)}}{I_{0(hkl)}}}{\frac{1}{N}\sum_N\left(\frac{I_{(hkl)}}{I_{0(hkl)}}\right)} \quad (10)$$

where $I_{(hkl)}$ integrated intensities corresponding to plane (hkl) in this study, $I_{0(hkl)}$ is integrated intensities theoretically, and N is the number of diffraction peak. It can be seen that the texture coefficient of plane is increase consistently shows that the crystalline of ZnO grew with plane (002)-oriented.

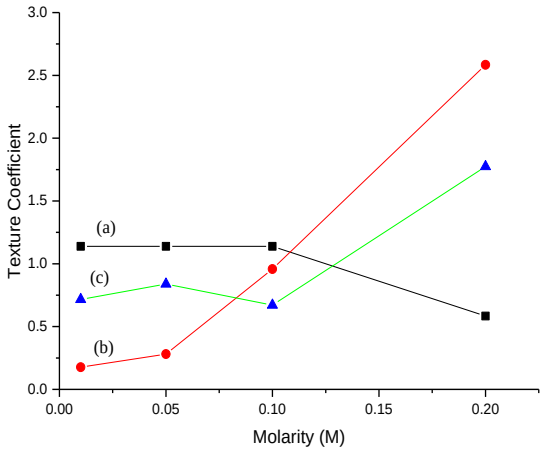

Figure 3. Texture Coefficient of ZnO nanostructures of (a) plane (100), (b) plane (002), (c) plane (101)

4 Conclusion

Flower-like ZnO nanostructures composed of nanoparticles were obtained at low molarity. It became more compact as the molarity increased. Flower-like composed of microrods were synthesized at 0.20 M. The crystallite size of 49.17 nm was consistent with other researcher findigs. The lattice constant “a” and “c” from XRD analysis were consistent with reference, JCPDS 36-1451. In addition, Zn-O bond to be 0.19 nm in all samples. The crystalline of ZnO grew with plane (002)-oriented based on texture coefficient analysis.

Acknowledgement: The authors would like to thank Universiti Teknologi MARA (UiTM) and also Malaysia Ministry of Higher Education for their support and funding from I-Rags Grant, file no: 600-RMI/IRAGS 5/3 (20/2015).

References

[1] J. G. Quiñones-Galván *et al.*, "Effect of precursor solution and annealing temperature on the physical properties of Sol–Gel-deposited ZnO thin films," *Results in Physics*, vol. 3, pp. 248-253, 2013/01/01/ 2013, doi: https://doi.org/10.1016/j.rinp.2013.11.001.

[2] M. Shaban, F. Mohamed, and S. Abdallah, "Production and Characterization of Superhydrophobic and Antibacterial Coated Fabrics Utilizing ZnO Nanocatalyst," *Scientific Reports*, vol. 8, no. 1, p. 3925, 2018/03/02 2018, doi: 10.1038/s41598-018-22324-7.

[3] K. Eswar *et al.*, "Hydrothermal growth of flower-like ZnO nanostructures on porous silicon substrate," *Journal of Molecular Structure*, vol. 1074, pp. 140-143, 2014.

[4] G. S. Devi, P. S. P. Reddy, and K. Ramya, "Sol-Gel Derived ZnO: Nb2O5 Nanocomposite as Selective Hydrogen (H2) Gas Sensor," *Materials Today: Proceedings*, vol. 3, no. 2, pp. 224-229, 2016/01/01/ 2016, doi: https://doi.org/10.1016/j.matpr.2016.01.061.

[5] K. A. Eswar, A. A. Azlinda, F. Husairi, M. Rusop, and S. Abdullah, "Synthesis of ZnO thin film on porous silicon by spin coating in various low molarities precursor," in *Advanced Materials Research*, 2013, vol. 701: Trans Tech Publ, pp. 167-171.

[6] S.-L. Ou, F.-P. Yu, and D.-S. Wuu, "Transformation from Film to Nanorod via a Sacrifical Layer: Pulsed Laser Deposition of ZnO for Enhancing Photodetector Performance," *Scientific Reports*, vol. 7, no. 1, p. 14251, 2017/10/27 2017, doi: 10.1038/s41598-017-14592-6.

[7] K. A. Eswar, F. S. Husairi, A. Ab Aziz, M. Rusop, and S. Abdullah. *Effect of post annealing temperature on surface morphology and photoluminescence properties of ZnO thin film, Advanced Materials Research*, vol. 832, pp. 654-658, 2014.

[8] K.-T. Lam, Y.-J. Hsiao, L.-W. Ji, T.-H. Fang, K.-H. Hsiao, and T.-T. Chu, "High-Sensitive Ultraviolet Photodetectors Based on ZnO Nanorods/CdS Heterostructures," *Nanoscale Research Letters*, journal article vol. 12, no. 1, p. 31, 2017, doi: 10.1186/s11671-016-1818-6.

[9] M. Husairi, J. Rouhi, K. Alvin, Z. Atikah, M. Rusop, and S. Abdullah, "Developing high-sensitivity ethanol liquid sensors based on ZnO/porous Si nanostructure surfaces using an

electrochemical impedance technique," *Semiconductor Science and Technology,* vol. 29, no. 7, p. 075015, 2014.

[10] K. A. E. M. M. Akhir, M. R. Mahmud, M. K. Harun, M. Rusop, S. Abdullah, "The Study of Structural and Corrosion Performance of ZnO Nanostructures Layer Coated on Mild Steel Surface," *Advanced Materials Research,* vol. 1109, pp. 405-409, 2015.

[11] K. Gao *et al.*, "Correlation between structure and photoluminescence of c-axis oriented nanocrystalline ZnO films and evolution of photo-generated excitons," *Solar Energy Materials and Solar Cells,* vol. 96, no. 1, pp. 117-123, 2012, doi: 10.1016/j.solmat.2011.09.033.

[12] A. Khorsand Zak, W. H. Abd. Majid, M. E. Abrishami, and R. Yousefi, "X-ray analysis of ZnO nanoparticles by Williamson–Hall and size–strain plot methods," *Solid State Sciences,* vol. 13, no. 1, pp. 251-256, 2011, doi: 10.1016/j.solidstatesciences.2010.11.024.

[13] J. Lee *et al.*, "Sputtered deposited nanocrystalline ZnO films: A correlation between electrical, optical and microstructural properties," *Applied Physics A,* vol. 80, no. 8, pp. 1641-1646, 2005.

[14] M. S. Kim *et al.*, "Growth and characterization of seed layer-free ZnO thin films deposited on porous silicon by hydrothermal method," *Electronic Materials Letters,* vol. 8, no. 1, pp. 75-80, 2012, doi: 10.1007/s13391-011-0130-y.

[15] S. K. Min *et al.*, "Nanocrystalline ZnO Thin Films Grown on Porous Silicon by Sol-gel Method and Effects of Post-annealing," *Journal of the Korean Physical Society,* vol. 59, no. 2, p. 346, 2011, doi: 10.3938/jkps.59.346.

[16] M. S. Kim, S. Kim, G. Nam, D.-Y. Lee, and J.-Y. Leem, "Effects of growth temperature for buffer layers on properties of ZnO thin films grown on porous silicon by plasma-assisted molecular beam epitaxy," *Optical Materials,* vol. 34, no. 9, pp. 1543-1548, 2012, doi: 10.1016/j.optmat.2012.03.024.

[17] M. S. Kim, K. G. Yim, S. Kim, G. Nam, and J.-Y. Leem, "White light emission from nano-fibrous ZnO thin films/porous silicon nanocomposite," *Journal of Sol-Gel Science and Technology,* vol. 59, no. 2, pp. 364-370, 2011, doi: 10.1007/s10971-011-2513-9.